Front. Optoelectron. 2017, 10(2): 166–173
DOI 10.1007/s12200-017-0710-z

RESEARCH ARTICLE

Off-axis two-mirror laser communication antenna designed using differential equations

Chunqiu XIA (✉)[1,2], Xing ZHONG[1,3]

1 Changchun Institute of Optics and Fine Mechanics, Chinese Academy of Sciences, Changchun 130033, China
2 University of Chinese Academy of Sciences, Beijing 100049, China
3 Chang Guang Satellite Technology Co. Ltd., Changchun 130033, China

Abstract In satellite laser communication technology, which is built between planets and between a planet and the Earth, the optical antenna is the key point. Thus, research on optical system design is important. The off-axis reflective system has no obscuration and hence possesses a high efficiency for energy transfer. This study proposes a novel method for designing a free-form off-axis reflective imaging system. This study also introduces differential equations that depend on Fermat's principle and sine condition. Finally, a free-form off-axis two-mirror optical system was designed by using the differential equation method. This system includes one intermediate image plane, in which the field of view (FOV) is $-5°$ to $-4°$ in the y-axis and $-1°$ to $0°$ in the x-axis. The modulation transfer function was greater than 0.7 at 50 lp/mm, and the efficiency of energy transmission was high. The free-form off-axis two-mirror optical system involves a wide range of application prospects in the optical antenna used in the satellite laser communication systems. Moreover, the design method that used differential equations was proven simple and effective.

Keywords optical antenna design, off-axis reflective system, satellite laser communication

1 Introduction

Satellite laser communication technology, which includes a laser as carrier, is a communication link with high speed and large capacity. This type of technology is built between planets and between a planet and the Earth. For point-to-point satellite laser communication, the optical antenna is the key point in satellite laser communication technology, which affects the laser link directly. Thus, research on optical system design is important [1].

Given the requirements of the launch cost, the working environment, and the working life, the performance of optical antenna terminals for satellite laser communication usually includes the following characteristics [2]. 1) The first characteristic is the high-efficiency energy transmission and reception. Satellite laser communication technology deals with the weak signal between remote distances, and the terminal is strictly limited by the satellite platform. Therefore, the transmitting and receiving systems are needed to achieve high-efficiency energy transmission. 2) Second, the receiving field of view (FOV) is larger than $1° \times 1°$. Satellite laser communication technology usually needs to complete the real-time dynamic laser communication between two high-speed laser communication terminals. Therefore, the receiving terminal is required to possess a large receiving FOV to improve the aiming and capturing efficiency. 3) The third attribute involves a high image quality. Although the optical antenna of satellite laser communication is a non-imaging system, the concentration of energy and the shape and size of the spot on the photodetector still significantly influences the transmission efficiency. 4) Lastly, the terminals are characterized by light weight, stable structure, and high reliability.

Generally, the reflective system is nondispersive and could handle a wide spectrum compared with the lens system. Thus, most laser commutation systems applied reflective systems, such as the Cassegrain reflective system. However, the traditional communication system (Fig. 1) includes a co-axis system, which has a central obstruction and hardly achieves a wide FOV and a high efficiency for energy transfer. At the same time, the traditional communication system needs lenses for imaging the beams at the detector. Theses lenses could bring in additional stray light to influence the efficiency of

Received March 6, 2017; accepted May 4, 2017

E-mail: chunq.xia@hotmail.com

communication. Therefore, the FOV with high efficiency for energy transfer of the traditional communication system is usually less than 1° .

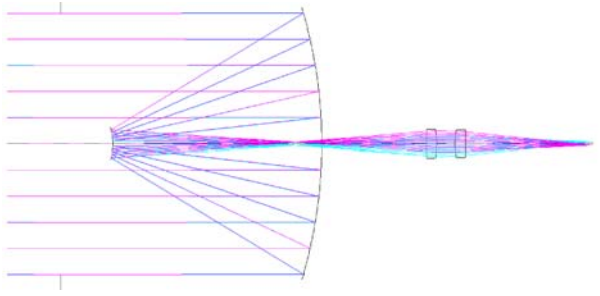

Fig. 1 Construction of the traditional communication system

On the basis of the deficiency of the traditional communication system, this study focuses on the off-axis reflective systems without lens. These systems include no obstruction and possesses a strong ability to eliminate stray light. Moreover, the off-axis reflective system without obstruction could handle a wide FOV. From the aforementioned reasons, the off-axis reflective system is a better alternative in satellite laser communication.

Nevertheless, a disadvantage of the off-axis mirror is the emergence of high-order aberration. Thus, additional designers apply the high degree of free-form surface to solve the aberration and reduce the number of mirrors [3–5]. The traditional design method was intended to symmetric and coaxial systems; after calculating the construction of the co-axis system, the reflective system was established by optimizing the off-axis mirror and the degree of free-form surfaces using the software Zemax or Code V [6–8]. However, the difference between initial co-axis construction and final off-axis system was relatively large that the optimization process usually wasted a considerable amount of time, and the optimal results were difficult to obtain.

Therefore, additional researchers focused their attention on the direct design method of the off-axis reflective system [9–11]. One important method was to establish the differential equations on the basis of the incident and exit rays, which determined the shape of the surfaces. The points on the surface can be calculated, and the free-form surfaces can be generated by surface fitting [12–14]. This design method is simple and effective in imaging optics. However, it is limited in its ability to manage only a single FOV of the system.

In this study, one off-axis two-mirror system with free-form surface was designed by using the improved differential equation method. The two-mirror system included one intermediate image plane, which attained the advantage to align and reduce stray light. At the same time, the number of mirrors was only two, such that the energy loss can be reduced. The improved design method initially determined the relationship between different ray bundles with different incident angles, as well as that of different imaging positions with different optical path lengths. Then, this method was used to calculate the one off-axis initial construction with free-form surface and multiple FOVs using differential equations, which depend on the sine condition and Fermat's principle. The initial construction was simply optimized for high imaging quality. Finally, this study designed one off-axis two-mirror system with a free-form surface, including one intermediate image plane, which achieved the FOV of $-5°$ to $-4°$ in the y-axis and $-1°$ to $0°$ in the x-axis, with a high efficiency for energy transmission.

2 Method

2.1 Principle of the differential equations

This section explains how the differential equations, which depend on Fermat's principle and sine condition, were established. First, the initial conditions, which included the entrance pupil, the position of the imaging points, and the sampling FOVs, were defined. Given that the satellite laser communication system operates in space, suppressing stray light, such as sunlight or reflected light from the Earth, is necessary. Therefore, the entrance pupil of the optical antenna is generally situated at the aperture before the system. The entrance pupil sets the positions of the starting points. Then, the directions of the rays emitted from the starting points of the entrance pupil are set. The construction of the entrance pupil is shown in Fig. 2. Figure 2(a) shows the uniform sampling points on the entrance pupil, and Fig. 2(b) shows the rays emitted from the points with different sampling FOVs. Each ray bundle with one direction arrives at an imaging point, where the positions of the corresponding imaging points are set.

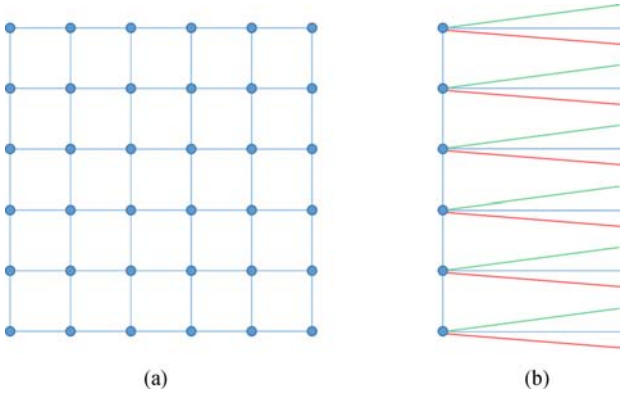

Fig. 2 Schematic of the points on the entrance pupil and the rays emitted from those points. (a) Uniform sampling points on the entrance pupil; (b) rays emitted from the points with different sampling FOVs

Figure 3(a) shows the diagram of one ray tracing between $n-1$ mirrors. The ray from the starting point (x_0, y_0, z_0) on the entrance pupil goes through $n-1$ mirrors and arrives at the imaging points (x_n, y_n, z_n).

The optical path length of one ray from the entrance pupil to the imaging points could be expressed as follows [1]:

$$w = \Sigma_0^n \sqrt{(x_k - x_{k-1})^2 + (y_k - y_{k-1})^2 + (z_k - z_{k-1})^2}. \quad (1)$$

Figure 3(b) shows that two rays form one starting point with different incident directions and finally arrive at different imaging points. In fact, the optical path lengths of the two rays are different. Notably, in the ray tracing process, all rays belonging to different FOVs correspond to different imaging points and different optical path lengths.

In this system, the ray arrived at the surface M_k on (x_k, y_k, z_k) and at the surface M_{k+1} on (x_{k+1}, y_{k+1}, z_{k+1}). From the Abbe sine condition, the relationship between the points (x_{k-1}, y_{k-1}, z_{k-1}), (x_k, y_k, z_k), and (x_{k+1}, y_{k+1}, z_{k+1}) [14] can be translated as follows:

$$\frac{z_{k+1}-z_k}{y_{k+1}-y_k} = \frac{\left(1-\frac{\partial y}{\partial z}\right)^2 (z_k - z_{k-1}) + 2(y_k - y_{k-1})\frac{\partial y}{\partial z}}{2(z_k - z_{k-1})\frac{\partial y}{\partial z} + (y_k - y_{k-1})\left(1-\frac{\partial y}{\partial z}\right)^2}, \quad (2)$$

$$\frac{z_{k+1}-z_k}{x_{k+1}-x_k} = \frac{\left(1-\frac{\partial x}{\partial z}\right)^2 (z_k - z_{k-1}) + 2(x_k - x_{k-1})\frac{\partial x}{\partial z}}{2(z_k - z_{k-1})\frac{\partial x}{\partial z} + (x_k - x_{k-1})\left(1-\frac{\partial x}{\partial z}\right)^2}. \quad (3)$$

The partial differential equations $\frac{\partial y}{\partial z}$ denote the tangential conic of mirror M_k, and $\frac{\partial x}{\partial z}$ denotes the sagittal conic of mirror M_k. $(z_{k+1}-z_k)/(y_{k+1}-y_k)$ denotes the direction of the ray from mirror M_k to mirror M_{k+1}. This equation indicates that the propagation of the ray between the mirrors M_k and M_{k+1} depends on the surface of M_k and the direction of the ray from the mirror M_{k-1} to the mirror M_k. If the surface M_{k+1} is an unknown surface, the surface M_{k+1} can be designed using Eqs. (1) to (3) by setting the mode of the differential equations as follows:

$$\begin{cases} \dfrac{z_{k+1}-z_k}{y_{k+1}-y_k} = \dfrac{\left[1-\left(\frac{\partial y}{\partial z}\right)^2\right](z_k - z_{k-1}) - 2(y_k - y_{k-1})\frac{\partial y}{\partial z}}{2(z_k - z_{k-1})\frac{\partial y}{\partial z} + (y_k - y_{k-1})\left[1-\left(\frac{\partial y}{\partial z}\right)^2\right]}, \\ \dfrac{z_{k+1}-z_k}{x_{k+1}-x_k} = \dfrac{\left[1-\left(\frac{\partial x}{\partial z}\right)^2\right](z_k - z_{k-1}) - 2(x_k - x_{k-1})\frac{\partial x}{\partial z}}{2(z_k - z_{k-1})\frac{\partial x}{\partial z} + (x_k - x_{k-1})\left[1-\left(\frac{\partial x}{\partial z}\right)^2\right]}, \\ w = \sum_0^n \sqrt{(x_{k+1}-x_k)^2 + (y_{k+1}-y_k)^2 + (z_{k+1}-z_k)^2}. \end{cases} \quad (4)$$

The differential equations (Eq. (4)) are three equations with the unknown factors x_k, y_k, z_k. The values of other parameters are provided, and the unknown factors are calculated as the position values of one point on the unknown surface M_{k+1}. The corresponding imaging points and corresponding optical path lengths of all incident rays were fitted to obtain the surface form.

2.2 Method used to design the off-axis two-mirror system with multiple FOVs

The laser commutation system is aimed at obtaining two free-form surfaces. For a two-mirror system, the information of the incident rays and imaging points of the first mirror is determined (Fig. 4(a)). In Fig. 4(a), two rays with different incident directions starting from (x_0, y_0, z_0) arrive at the known surface (x_{11}, y_{11}, z_{11}) and (x_{12}, y_{12}, z_{12}). These rays can be reflected on the next unknown surface (x_{21}, y_{21}, z_{21}) and (x_{22}, y_{22}, z_{22}) and then arrived at their

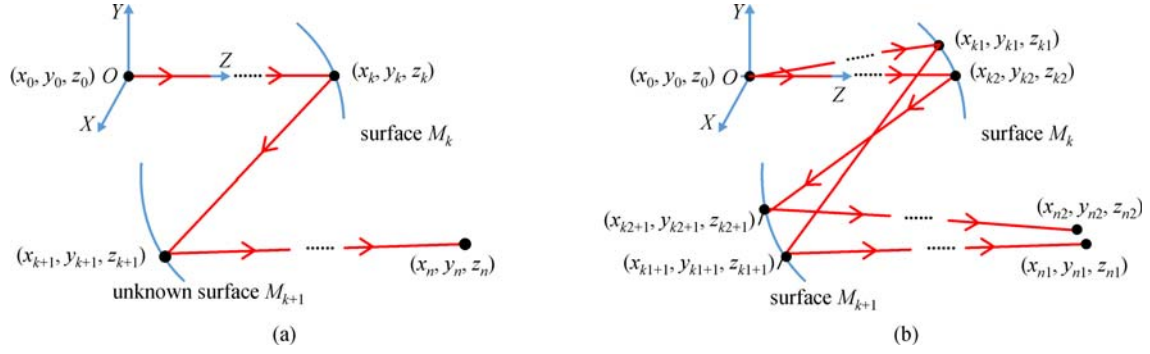

Fig. 3 Schematic of one ray tracing between $n-1$ mirrors. (a) Diagram of one ray tracing between $n-1$ mirrors; (b) two rays form one starting point with different incident directions and finally arrive at different imaging points

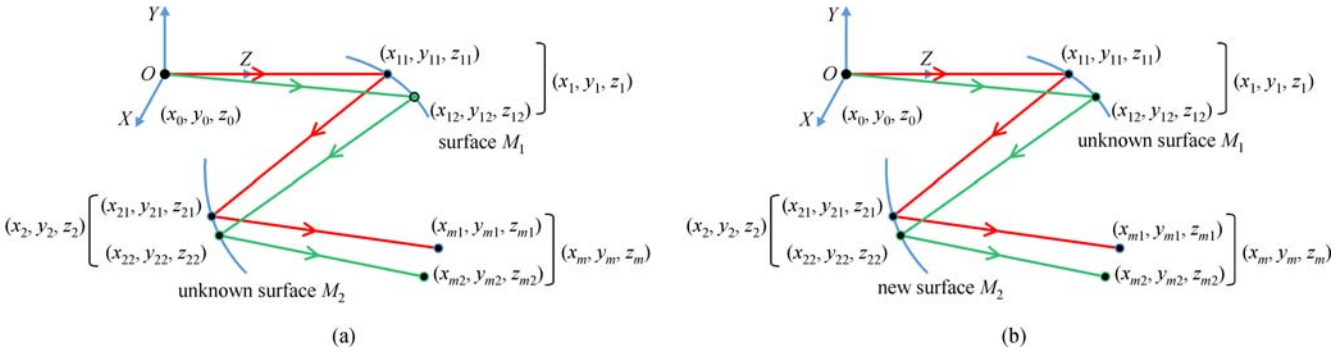

Fig. 4 Diagram of ray tracing between two mirrors. (a) M_2 is an unknown surface; (b) M_1 is an unknown surface with a new M_2

corresponding imaging points (x_{m1}, y_{m1}, z_{m1}) and (x_{m2}, y_{m2}, z_{m2}). We designed the M_2 first depending on the initial condition, and then designed the new M_1 depending on the new surface M_2. The entire workflow is shown in Fig. 5.

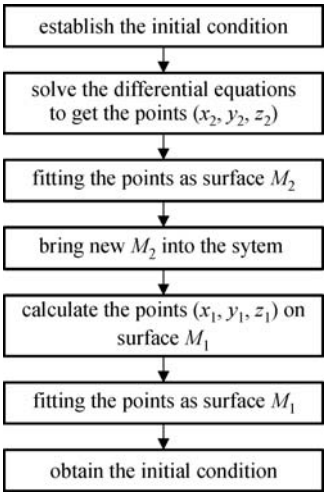

Fig. 5 Workflow of the design process for two mirrors

The steps are described as follows. ① The original initial structure, such as the sampling FOV, the initial surface form of M_1, and the different imaging points (x_m, y_m, z_m) with different sampling FOVs, was set. ② The initial conditions, including the points (x_1, y_1, z_1) and the optical path length $\boldsymbol{w}$ with different FOVs, were calculated with the optical path length $\boldsymbol{w}$. In the process, the position of the unknown surface was determined, and the value was calculated depending on where the surface should be situated. ③ The points (x_2, y_2, z_2) on surface M_2 was calculated using the differential equation expressed in Eq. (5). ④ The surface M_2 was fitted using the points (x_2, y_2, z_2). When the second mirror is known, the information of the incident rays and imaging points (Fig. 3(b)) and the starting positions and incident directions of the incident rays (Eqs. (6) and (7)) exhibit the relationship between the values of x_1 and x_2. ⑤ The new surface M_2 was brought into the two-mirror system, and the value of z_1 of the new surface M_1 was calculated using (x_2, y_2, z_2) and the starting points (x_0, y_0, z_0) and imaging points (x_m, y_m, z_m) using the optical path lengths. The values of x_1 and x_2 were calculated using Eqs. (6) and (7). ⑥ The surface M_1 was fitted using points (x_1, y_1, z_1), and the new initial construction of the two-mirror system with free-form surface was obtained. ⑦ The initial construction for high imaging quality was also optimized. In this process, the points could be fitted for the free-form surface, such as Zernike polynomial or x–y polynomial.

$$\left\{\begin{aligned}
&\frac{z_2-z_1}{y_2-y_1}=\frac{\left(1-\dfrac{\partial y}{\partial z}\right)^2(z_2-z_0)+2(y_1-y_0)\dfrac{\partial y}{\partial z}}{2(z_1-z_0)\dfrac{\partial y}{\partial z}+(y_1-y_0)\left(1-\dfrac{\partial y}{\partial z}\right)^2}\\
&\frac{z_2-z_1}{x_2-x_1}=\frac{\left(1-\dfrac{\partial x}{\partial z}\right)^2(z_1-z_0)+2(x_1-x_0)\dfrac{\partial x}{\partial z}}{2(z_1-z_0)\dfrac{\partial x}{\partial z}+(x_1-x_0)\left(1-\dfrac{\partial x}{\partial z}\right)^2}\\
&w=\sum_0^n\sqrt{(x_k-x_{k-1})^2+(y_k-y_{k-1})^2+(z_k-z_{k-1})^2}
\end{aligned}\right\}, \tag{5}$$

$$x_1=x_0+(z_1-z_0)*\arcsin(x_{\mathrm{FOV}}/\cos(y_{\mathrm{FOV}})), \tag{6}$$

$$y_1=y_0+(z_1-z_0)*\arcsin(y_{\mathrm{FOV}}). \tag{7}$$

In Eqs. (6) and (7), the x_{FOV} and y_{FOV} denote the projection plane of the included angles between the incident ray and the z-axis in the YOZ and XOZ planes, respectively.

2.3 System parameters and the initial condition

Given the requirements of optical antenna terminals for satellite laser communication, the parameter sets of this system are given in Table 1.

Given the parameter requirements listed in Table 1, the system with intermediate image plane surface possesses the advantage of eliminating stray light and aligns the satellite laser communication system. For easy installation

Table 1 Parameters of the optical antenna for satellite laser communication

Parameters	specification
FOV	−5° to −4° in the *y*-axis and −1° to 0° in the *x*-axis
diameter of the entrance pupil	100 mm
distance between the entrance pupil and the image plane	400 mm
efficiency of energy transmission	higher than 90% at the 20 μm imaging spots
geometric imaging spots	diameter is less than 50 μm

of the system, the initial conditions are set as follows:

1) The size of the entrance aperture is 100 mm.

2) The FOVs are (0°, −5°), (0°, −4°), (−0.5°, −5°), (−0.5°, −4°), (−1°, −5°), and (−1°, −4°).

3) The distance of the entrance aperture from the first mirror or the second mirror is 400 mm.

4) If the system is a two-mirror system with intermediate image plane, the distance of M_1 and M_2 should be larger than the focal length of M_1. Thus, the initial radius of M_1 should satisfy this condition.

The radius of the first mirror was set as −400 mm, decentered by −100 mm in the *y*-axis, and expressed as follows:

$$z = \frac{c[x^2 + (y+100)^2]}{1 - \sqrt{(1+k)c^2[x^2 + (y+100)^2]}}, \quad (c = -400,\ k = -3). \tag{8}$$

The initial conditions only provide the position and relationship of the two mirrors, and distributing the focal power of M_2 is unnecessary. M_2 is set as the plane mirror without tilt. The diagram of the initial conditions is shown in Fig. 6.

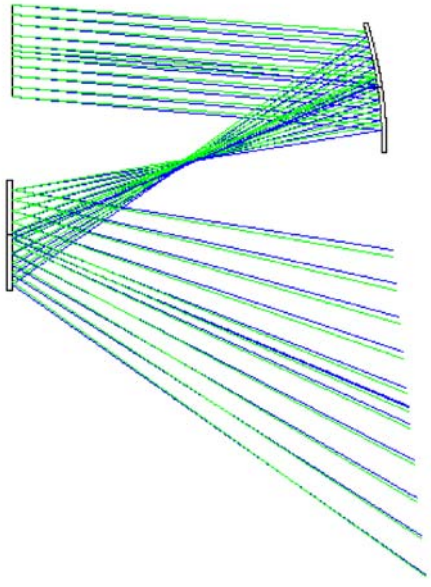

Fig. 6 Diagram of the initial conditions of the two-mirror system

5) The imaging positions are (0, −160, 400), (0, −150, 400), (4, −160, 400), (4, −150, 400), (8, −160, 400), and (8, −150, 400).

6) The optical lengths are 1265, 1257, 1250, 1242, 1236, and 1227 mm.

3 Results and discussion

Figure 7 shows the results of the calculation of the differential equations, where Fig. 7(a) shows the calculated points of M_2, and Fig. 7(b) shows the calculated points of M_1. After surface fitting, the initial two-mirror system was obtained using the *x*–*y* polynomial.

$$z = p1 + p2*x + p3*y + p4*x^2 + p5*x*y + p6*y^2 + p7*x^3 + p8*x^2*y + ... \tag{9}$$

The surface expression is given in Eq. (9). The system with limitations on the positions of the imaging points was optimized for better imaging quality in the software Code V. The parameters of the final system are shown in Table 2. The surfaces of M_1 and M_2 were *x*–*y* polynomial surface types. The *x*–*y* polynomial surface could be tested using the computer-generated hologram method [15], which can achieve high-precision detection of free-form surfaces and has a wide range of application prospects. The construction of the optimized system is shown in Fig. 8.

Given that the performance of space laser communication is mainly related to the efficiency of energy transmission and the wave front quality, the imaging spots, the modulation transfer function (MTF), and the diffraction encircled energy were used as parameters for the performance evaluation method. Figure 9 shows the MTF curve of this system. The MTF of the final system was greater than 0.7 at 50 lp/mm and approached the diffraction limit. Thus, the imaging quality satisfied the requirements of laser communication. Figure 10 shows the spot diagram of the sampling FOV. All RMS were less than 7 μm, and the radius of 100% geometrical spots were less than 13 μm, meeting the requirements of laser communication. Table 3 shows the distribution of diffraction encircled energy, and when the efficiency of energy transfer was 90%, the diameters of the circles of all FOVs were less than 13 μm. The results of the free-form

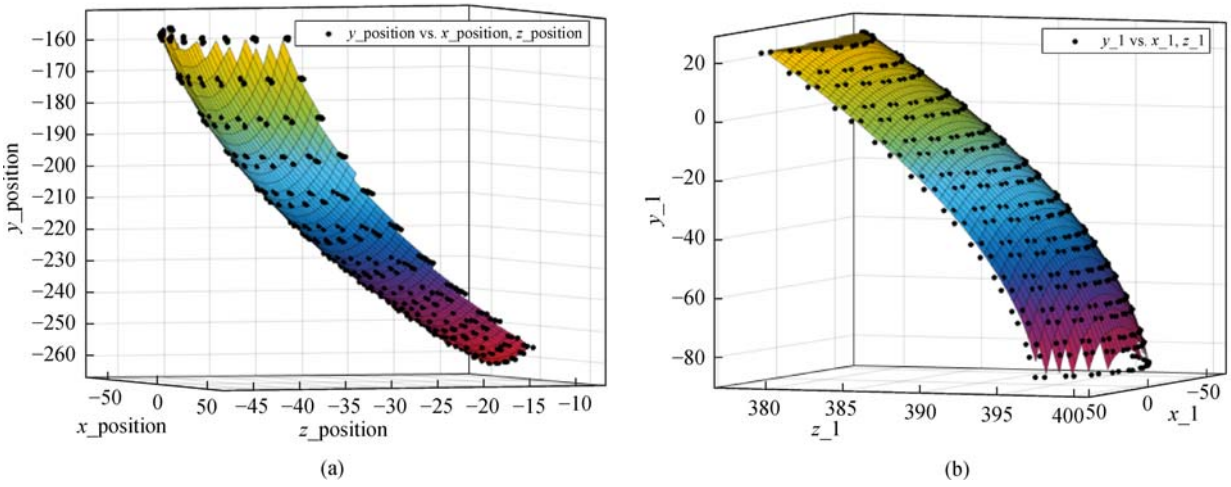

Fig. 7 Results of the calculation of the differential equations. (a) Points on M_2 calculated using the differential equations; (b) points on M_1 calculated using the differential equations

Table 2 Final construction of M_2

type	M_1	M_2
position/mm	400	−13.8081
X	−0.0101780682945791	0.0218755242575204
Y	−0.18778755243862	0.310394559158681
X^2	−0.00140634100279195	0.00164599920358782
XY	7.40989422792883e−006	2.37286235345416e−005
Y^2	−0.00137183287985337	0.00181687918117691
X^3	1.99906773762904e−008	1.13658182868091e−007
X^2Y	3.41306778799434e−009	1.6843233366858e−006
XY^2	2.02348777306767e−008	1.78683536317886e−007
Y^3	−4.73230885524817e−009	1.98757830856979e−006
X^4	−1.32168346394334e−009	4.06208751422954e−009
X^3Y	2.89312385059487e−011	3.78983199531588e−010
X^2Y^2	−2.51065003043903e−009	1.16899196243512e−008
XY^3	4.08432779113874e−011	5.22623915732657e−010
Y^4	−1.35471359891913e−009	7.84826112392608e−009
X^5	6.45843781562083e−014	7.13864490652392e−013
X^4Y	5.89221403345031e−013	1.2489373339076e−011
X^3Y^2	4.24405464367715e−013	1.86632949847675e−012
X^2Y^3	1.5669170279279e−012	2.92561406404347e−011
XY^4	4.80712856308573e−013	1.32045372324571e−012
Y^5	−6.62286432667559e−013	1.58797601008602e−011
…	…	…

off-axis reflective imaging system prove that the differential equation method could be used to design the optical antenna for satellite laser communication with high imaging quality and efficiency of energy transfer.

In addition, the FOV is asymmetric with respect to the x- and y-axes, and the software Code V did not provide a correct distortion curve. Thus, the relative distortion in the y-axis was calculated by real ray tracing and ideal optical calculation to investigate whether the distortion of this free-form off-axis system can affect laser transmission.

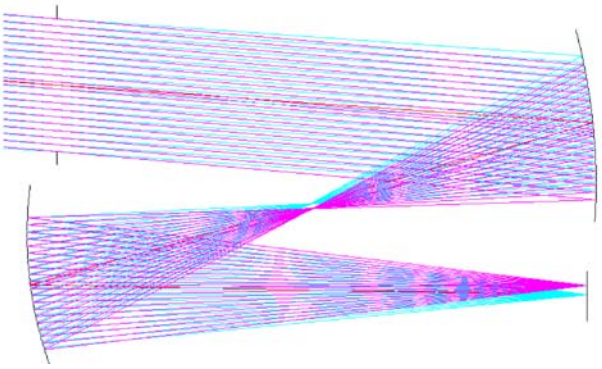

Fig. 8 Final construction of the off-axis two-mirror system

The distortion of the off-axis system can be expressed as follows [16]:

$$\sigma = \frac{y_w \cos\theta}{f * \tan w} - 1. \quad (10)$$

In Eq. (10), y_w denotes the real imaging height, θ denotes the off-axis angle of the light beam incident to the focal plane, w denotes the incident angle, and f denotes the focal length.

Table 3 Distribution of diffraction encircled energy

FOV	diameter of the circle/μm
(−1°, −5°)	12.824
(−1°, −4°)	12.961
(0°, −5°)	12.758
(0°, −4°)	12.681
(−0.5°, −5°)	9.0993
(−0.5°, −4°)	9.3251

The results of real ray tracing and focal length are shown in Table 4.

Depending on the values presented in Table 4 and Eq. (10), the relative distortions of −5° and −4° FOVs in the y-axis were 0.25% and 0.14%, respectively. These results showed that the distortions of this system had only a slight influence on laser communication.

4 Conclusion

This study proposed one off-axis two-mirror system with free-form surface and intermediate image plane for the optical antenna for satellite laser communication depending on the improved differential equations. In this method, mapping between different FOVs and different imaging points and the positions and status of the mirrors were set by the designer in advance by simplifying the off-axis and optimization processes. The free-form off-axis two-mirror optical system designed using this method has a large FOV and a high efficiency for energy transfer with only a few mirrors. The MTF of this system was greater than 0.7 at 50 lp/mm, which is close to the diffraction limit. When the efficiency of energy transfer was 90%, the diameters of the circles of all FOVs were less than 13 μm, satisfying the requirements of laser communication. Therefore, this kind of off-axis two-mirror system with multiple FOVs designed using differential equations for the optical antenna for satellite laser communication, which will involve a wide range of application prospects.

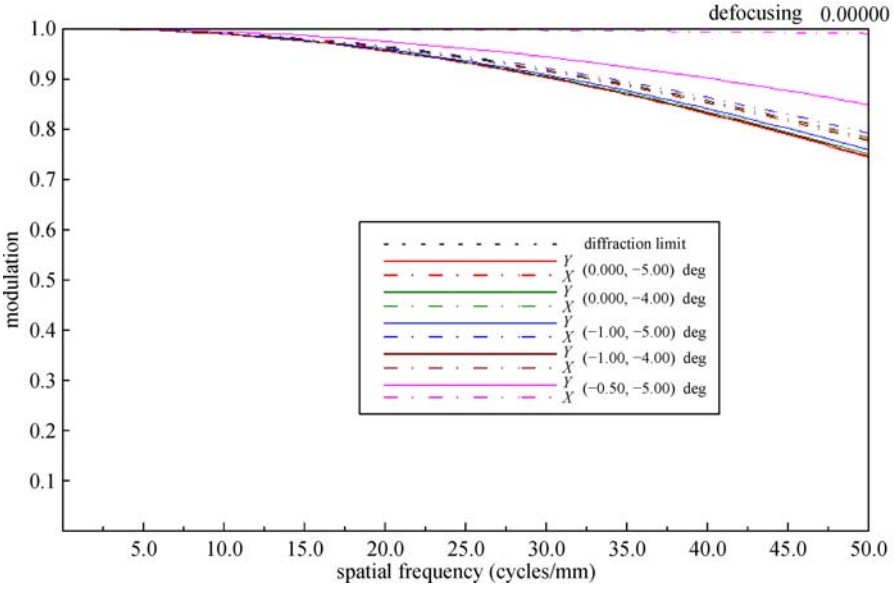

Fig. 9 MTF of the final system

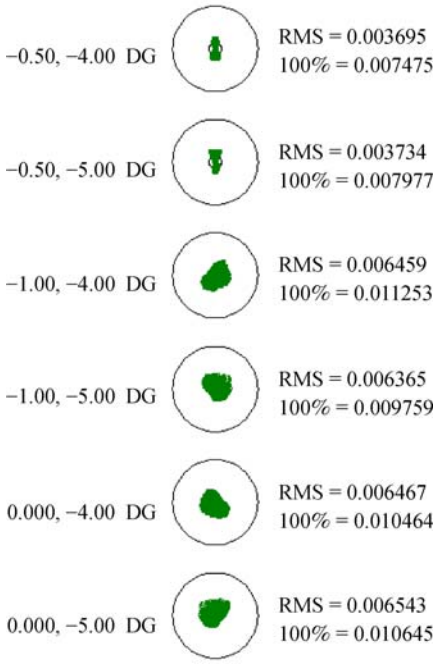

Fig. 10 Spot diagram of the satellite laser

Table 4 Results of real ray tracing and focal length

parameter	value
focal length	−540 mm
height of the imaging points of −5° FOV	−150
height of the imaging points of −4° FOV	−159.441
value of θ of −5° FOV	2.5°
value of θ of −4° FOV	1.14°
relative incident angle w	1°

Acknowledgements This study was supported by the Youth Innovation Promotion Association, Chinese Academy of Sciences and the National Science Foundation for Young Scholars of China (Grant No. 61505203).

References

1. Zhang Z, Xin Y, Yang B. The application of self-adaptation optics on space optical sensors. Spacecraft Recovery of Remote Sensing, 2000, 10(3): 23–29
2. Duchmann O, Planche G. How to meet intersatellite links mission requirements by an adequate optical terminal design. Proceedings of the Society for Photo-Instrumentation Engineers, 1991, 1417: 30–41
3. Xing Z, Guang J. Design of extra wide short wave infrared spectral imager's fore-optics. Acta Optica Sinica, 2012, 32(10): 1022004
4. Rodgers J M. Unobscured mirror designs. Proceedings of the Society for Photo-Instrumentation Engineers, 2002, 4832: 33–60
5. Rodgers J M. Aberrations of unobscured reflective optical systems. Dissertation for the Doctoral Degree. Tucson: University of Arizona, 1983
6. Hui L, Li X, Pei Y, Ming P. Design of off-axis three-mirror optical system. Laser & Optoelectronics Progress, 2008, 10(12): 59–63
7. Guo Y, Li Y, Liang T, Chen Q. Optical design of the uncoaxial three-mirror system with wide field of view. Acta Optica Sinica, 2010, 30(9): 2680–2683
8. Wu H, Wang P. Designs of reflective off-axis system. Opto-Electronic Engineering, 2006, 33(1): 34–37
9. Yang T, Zhu J, Jin G. Design of freeform imaging systems with linear field-of-view using a construction and iteration process. Optics Express, 2014, 22(3): 3362–3374
10. Yang T, Zhu J, Wu X, Jin G. Direct design of freeform surfaces and freeform imaging systems with a point-by-point three-dimensional construction-iteration method. Optics Express, 2015, 23(8): 10233–10246
11. Nie Y, Thienpont H, Duerr F. Multi-fields direct design approach in 3D: calculating a two-surface freeform lens with an entrance pupil for line imaging systems. Optics Express, 2015, 23(26): 34042–34054
12. Shealy D L, Wang C, Jiang W, Jin L, Hoover R B. Design and analysis of a fast two-mirrorsoft-x-ray microscope. In: Proceedings of SPIE- The International Society for Optical Engineering, 1992, 1741
13. Semin V A. Calculating aspheric surfaces by modelling an optical system by means of differential equations. Journal of Optical Technology, 1999, 66(3): 247–251
14. Xia C Q, Xing Z, Guang J. Design of the off-axis four mirrors system by differential equations. Acta Optica Sinica, 2015, 35(9): 0922002
15. Meng Q, Wang W, Ma H, Dong J. Easy-aligned off-axis three-mirror system with wide field of view using freeform surface based on integration of primary and tertiary mirror. Applied Optics, 2014, 53(14): 3028–3034
16. Guo J, Sun J, Shao M, Hu H. Calculation of focal length for off-axis TMA aerospace mapping camera. Optics and Precision Engineering., 2012, 20(8): 1754–1758

Chunqiu Xia obtained her Bachelor's degree from the Ocean University of China and majored in optoelectronic information technology from 2008 to 2012. She was a Ph.D. student in Changchun Institute of Optics and Fine Mechanics and majored in optical engineering from 2012 to 2017. Her research areas are optical system design and testing.

Xing Zhong is a professor and a doctoral supervisor in the Chinese Academy of Sciences. He is also the satellite system chief designer in Chang Guang Satellite Technology Co., Ltd. His main research interests include optical system design, optical inspection, optical navigation system, and optical measurement.